JOURNAL OF CHEMICAL INFORMATION AND MODELING

Article

pubs.acs.org/jcim

Murine mPGES-1 3D Structure Elucidation and Inhibitors Binding Mode Predictions by Homology Modeling and Site-Directed Mutagenesis

Gaia Corso,*[,†] Isabella Coletta,[‡] and Rosella Ombrato*[,†]

R&D, [†]Computational Chemistry Lab, [‡]In vitro Pharmacology Dev., Angelini Research Center, ACRAF S.p.A. P.le della Stazione, snc, I-00040 Santa Palomba, Pomezia (RM), Italy

Supporting Information

ABSTRACT: Microsomal prostaglandin E synthase-1 (mPGES-1) constitutes an inducible glutathione-dependent integral membrane protein that catalyzes the oxido-reduction of cyclooxygenase derived PGH_2 into PGE_2. mPGES-1 is an essential enzyme involved in a variety of human diseases or pathological conditions, such as rheumatoid arthritis, fever, and pain; it is therefore regarded as a primary target for development of next-generation anti-inflammatory drugs. Several compounds targeting human mPGES-1 have been reported in the literature. However, none of them is really specific for mPGES-1, and quite surprisingly, all of these compounds have very low or no activity against murine mPGES-1, making preclinical development hard and very expensive. In order to overcome this unresolved question, the current study focuses on the elucidation of the molecular determinants of murine mPGES-1 ligand binding modes combining protein homology modeling and site-directed mutagenesis approaches. We have developed, for the first time, two murine mPGES-1 models, describing both the closed and the open/active conformation of the enzyme. The 3D structure of human mPGES-1 having been recently disclosed, the main differences between the human and the murine enzyme models are described, emphasizing the smaller dimensions of the rodent substrate binding site, which could account for different activity of a ligand toward the two species. Furthermore, active binding modes are hypothesized, highlighting the most likely important residues for inhibition activity, whose identification is supported by *in-house* mutagenesis experiments. The results of our work could provide grounds for a rational structure-based drug design aimed to identify new inhibitors active against both human and murine mPGES-1.

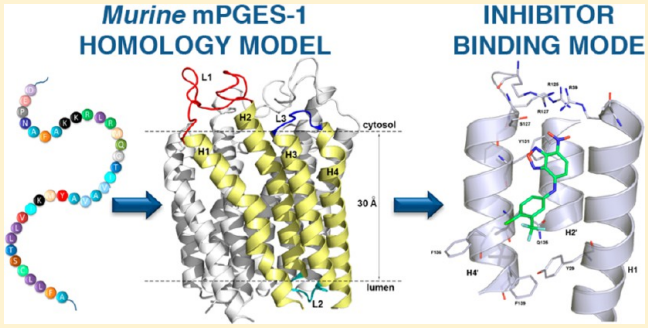

INTRODUCTION

Microsomal prostaglandin E synthase-1 (mPGES-1) is an inducible, glutathione (GSH) dependent enzyme that acts downstream of cyclooxygenases (COX-1/2) and specifically catalyzes the isomerization of prostaglandin PGH_2 to PGE_2 (Figure 1 illustrates the arachidonic acid cascade), most prominently in inflammatory conditions. mPGES-1 was originally termed MGST1-L1 because microsomal glutathione transferase 1 (MGST-1), a 17.3 kDa/subunit homotrimeric enzyme belonging to the membrane associated proteins in the eicosanoid and glutathione metabolism (MAPEG) superfamily, is its closest homologue, with 38% sequence identity.[1]

Different gene products with PGES activity have been cloned to date, namely, PTGES1, PTGES2, and PTGES3, encoding microsomal PGES-1 (mPGES-1), PGES-2 (mPGES-2), and cytosolic PGES (cPGES), respectively. mPGES-1 expression is typically induced by pro-inflammatory stimuli, whereas it is maintained at minimal levels in most normal tissues, although abundant and constitutive expression is detected in a limited number of organs, such as lung, kidney, and reproductive organs.[2] mPGES-2 is expressed constitutively in a variety of human tissues. Unlike mPGES-1, it is not induced by pro-inflammatory signals, and it is synthesized as a Golgi membrane-associated protein.[3] cPGES is also expressed in an ubiquitous manner under basal conditions. It is localized in the cytosolic region, and it is thought to mediate constitutive PGE_2 biosynthesis based on its preferential coupling with COX-1 for the maintenance of homeostasis.[4] PGE_2 is a lipid mediator with a key role both in many physiological processes, including gastrointestinal and renal functions, vascular homeostasis, bone remodelling, fever induction, and pregnancy, and under pathological conditions,[5] such as inflammation, anorexia, atherosclerosis, stroke, pain response, and cancer.[6] The relevance of mPGES-1 in the control of inflammation-induced PGE_2 production was demonstrated in mPGES-1-deficient mice that exhibited reduced inflammatory responses and inflammatory pain in a model of collagen-induced arthritis, suggesting that mPGES-1 is involved in acute and chronic inflammation.[7] Moreover, experiments on mPGES-1-deficient

Received: March 27, 2013
Published: June 22, 2013

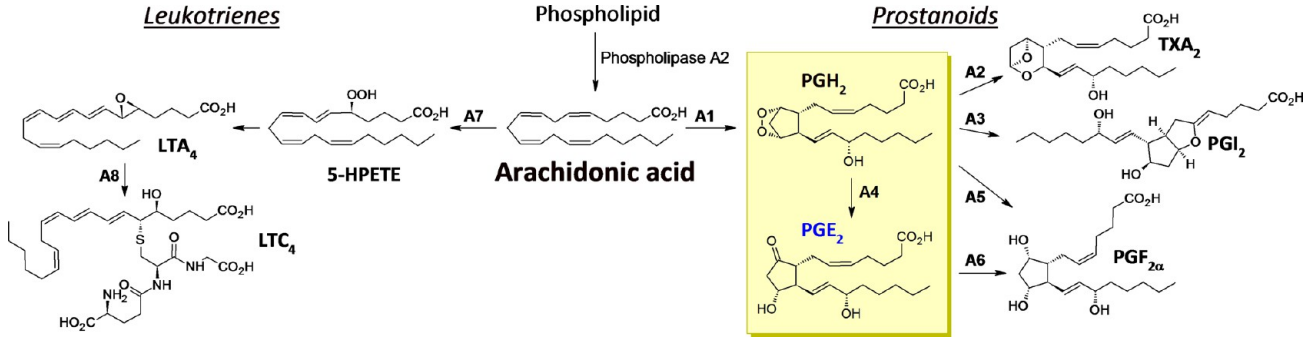

Figure 1. Arachidonic acid cascade. The reaction catalyzed by mPGES-1 is in the yellow colored boxed. A1: PGH synthase (cyclooxygenase), A2: TXA_2 synthase, A3: PGI_2 synthase, A4: PGE_2 synthase (cPGES, mPGES-1, mPGES-2), A5: $PGF_{2\alpha}$ synthase, A6: PGE_2 to $PGF_{2\alpha}$ reductase, A7: 5-LOX, A8: LTC_4S.

Table 1. Available 3D Structures for Members of MAPEG Superfamily

MAPEG	X-ray PDB code	resolution (Å)	available	year	ref.
h-mPGES1	3dww (2D crystal)	3.5	yes	2008	19,23
h-mPGES1		10.0	no	2003	24
r-MGST1	2h8a (2D crystal)	3.2	yes	2006	18c
h-LTC_4S	2uuh, 2uui, 2pno	2.2, 2.0, 3.3	yes	2007	22b,22a
h-FLAP	2q7m, 2q7r	4.3, 4.0	yes	2007	25

mice showed consistent reduction in both the number and size of intestinal tumors[8] and of a Lewis lung carcinoma cell xenograft.[9]

Although inhibition of COX-2 is an effective way to shut down the production of induced pro-inflammatory PGE_2, thus preventing the symptoms of inflammation like pain and fever, the use of cyclooxygenase-2 inhibitors (COXIBs) has been limited because of their adverse side effects on the cardiovascular system. In vascular endothelial cells along with PGI2 synthase, COXIBs suppress production of antithrombotic PGI2 (as measured by its stable urinary metabolite 2,3-dinor-6-keto PGF1α) to a similar degree as with traditional nonselective NSAIDs. In contrast to these isoform unspecific NSAIDs, however, COXIBs do not affect levels of COX-1 derived TXA_2 and fail to inhibit platelet aggregation *ex vivo*. Thus, the use of COXIBs removes a protective constraint on thrombogenesis, hypertension, and atherogenesis *in vivo*.[10−12] The interest has therefore shifted to enzymes downstream of the COXs, such as mPGES-1, as potential targets for novel, anti-inflammatory, and anticancer interventions without the undesired side effects due to COX-2 inhibition.[6,8,9] mPGES-1 is a terminal prostaglandin synthase, not coupled to any downstream enzymes in the arachidonic acid cascade. Furthermore, constitutive levels of mPGES-1 are normally low, and mPGES-1 is highly up-regulated by pro-inflammatory stimuli. Therefore, it is generally regarded as a promising target for pharmaceutical intervention of inflammatory conditions with a reduced risk of severe side effects.[6b] Recently, several mPGES-1 inhibitors have been identified in experimental screening efforts.[13] Some of these compounds potently inhibit human mPGES-1 with IC_{50} values in the submicromolar range but do not have any effects on the rodent orthologous, making preclinical development hard and very expensive.

mPGES-1 is one of the six members of the MAPEG superfamily (Membrane Associated Proteins in Eicosanoid and Glutathione metabolism), all of them being extensively distributed in eukaryotes and prokaryotes, but not found in archaea.[14] These six transmembrane proteins have highly different functions:[15] the two members leukotriene C4 synthase (LTC_4S)[16] and 5-lipoxygenase activating protein (FLAP)[17] are essential for the production of arachidonic acid-derived messengers; the microsomal glutathione S-transferase 1 (MGST-1) is mostly involved in the oxidative stress response and xenobiotic detoxification,[18] while the two homologues MGST-2 and MGST-3 have relatively broad substrate specificity and overlapping activities with LTC_4S and MGST-1, even if little is known about their *in vivo* functions.[6b] GSH is the cofactor for all MAPEG proteins, and MAPEG members sequence similarities showed conservation among the most important GSH-binding residues.[14a] Furthermore, the U-shaped GSH conformation in the LTC_4S 3D structure is supposed to be conserved among the other MAPEG proteins,[14a] as demonstrated in the 3.5 Å in-plane resolution 3D structure of *human apo* mPGES-1.[19] This *apo* structure was crystallized only with the cofactor, and it likely describes the closed conformation of the enzyme, which presumably is inactive.[19] In the assumed open conformation of mPGES-1 (catalytically competent), H1 is bent, leaving greater space in the predicted binding site, allowing also the endogen substrate PGH_2 to be accommodated.[19] H1 could indeed participate in a dynamic equilibrium allowing opening/closing of the binding site: its high flexibility has been confirmed for the homologue MGST-1 by hydrogen/deuterium exchange dynamics,[20] and it decreases for the presence of a hydrophobic ligand.[21] In the LTC_4S 3D structure,[22] the substrate binding site is hypothesized to be localized into neighboring subunits, and it was proposed that in the mPGES-1 3D structure, the PGH_2 binding site is localized in an analogous region.[14a] All the available 3D structural data of the MAPEG members are reported in Table 1, and to the best of our knowledge no murine mPGES-1 3D structure has been published, nor has any homology model been built. Many active compounds against human mPGES-1 have been reported in the literature, as recently reviewed,[13] but only a few known compounds showed weak μM activity against the murine enzyme (MK886, compound **1**,[26] and compound **2**[27] in Figure 2, which have been tested in house, data not

dx.doi.org/10.1021/ci400180f | J. Chem. Inf. Model. 2013, 53, 1804−1817

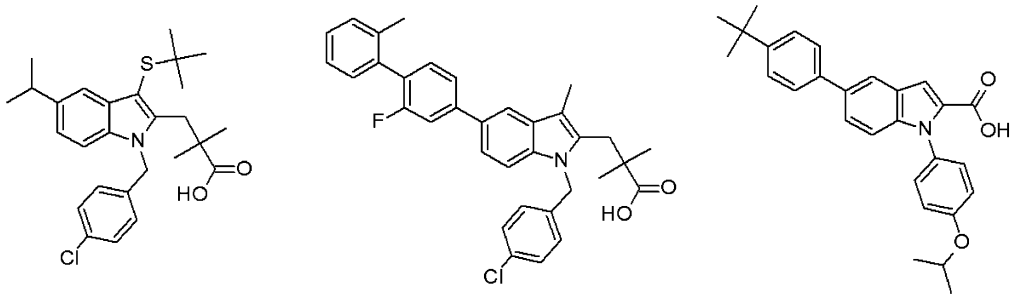

Figure 2. Chemical structures of three compounds from Merck and Biolipox showing weak μM activity against the murine mPGES-1.

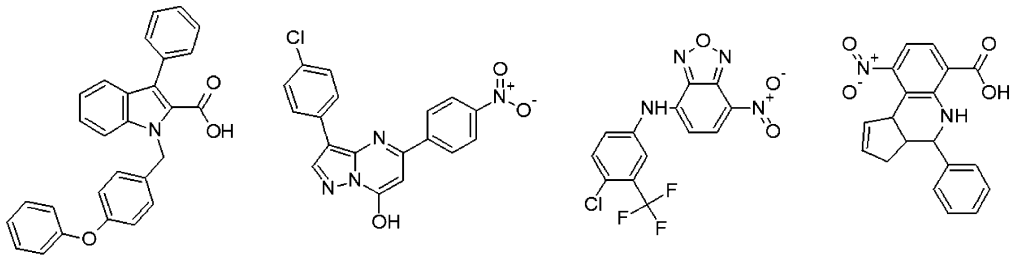

Figure 3. Chemical structures of corporate (compound **3**) and commercial compounds (compounds **4**–**6**) showing weak activity against murine mPGES-1.

shown). Furthermore, we identified some murine mPGES-1 weak active compounds from the corporate database (e.g., compound **3** in Figure 3) and the ChemBridge commercial libraries (compounds **4**–**6** in Figure 3); their percent inhibitions at 50 μM are reported in Table S1 in the Supporting Information. Recently, several compounds active against both the human and the rat enzymes have been published,[28] and a poorly described and not published homology model of the rat mPGES-1 has been developed[29] (mouse–rat mPGES-1 sequence identity 98%). Loss of activity against the rodent enzyme makes preclinical development harder and much more expensive than usual, since transgenic rodents or other mammals have to be used (as with the case of MF63 developed by Merck using guinea pigs[30]). For this reason, many scientists involved in the study of mPGES-1 focused on the identification of compounds active against both the human and the rodent enzymes. In the past decade, Angelini's efforts in inflammatory diseases led to the identification of potent inhibitors of human mPGES-1.[31] Aimed at identifying potent human/murine mPGES-1 inhibitors, the homology modeling technique could be applied to the murine enzyme, allowing us to build a 3D model and to elucidate the main differences between the murine and the human enzymes. Furthermore, a hypothesis on the binding mode of all the available active compounds into the murine 3D structure is described because it could be helpful for future virtual screening studies and identification of murine mPGES-1 hit compounds, which could then acquire also the activity against the human enzyme by taking advantage of our wide knowledge about the SAR of human mPGES-1 inhibitors.

MATERIALS AND METHODS

All the images illustrated in the present work were obtained using the software PyMOL.[32]

Computational Methods. *Homology Models Building.* The murine mPGES-1 sequence (UniProtKB ID: PTGES_MOUSE) was downloaded from the UniProtKB Web site,[33] and the template structures (human mPGES-1, PDB 3DWW, and human LTC_4S, PDB 2UUH) were downloaded from the RCSB-PDB.[34] The multiple sequence alignment and the homology modeling steps were performed using the software Prime.[35] In the present work, a conservative approach was adopted, without significantly altering the output 3D structure. The GSH pose was added to the 3D structure murine mPGES-1 model by superimposition with the LTC_4S-GSH template. Before submitting to Prime Refinement, the homology models were prepared with the Schrödinger Protein Preparation Wizard[36] (see below in the Ligand and Protein Preparation section). In the prime refinement step, for loop and side-chain refinement, the solvent was treated implicitly setting the dielectric constant values for the protein interior and the external parts to 1.0 and 80.0, respectively. The truncated-Newton energy method was the choice for minimization, using the OPLS_2005 all-atom force field for proteins as well as for the cofactor and treating solvation energies and effects via the Surface Generalized Born (SGB) continuum solvation model. The homology models' reliability was evaluated by Ramachandran plots and the Schrödinger protein reports (analyzing the steric clashes, the bond length and bond angle deviation, the backbone and side-chain dihedrals, the G-factor summary, the average and the gamma-atom B-factor, the peptide and side-chain planarity, the C-alpha stereochemistry, and the missing atoms[37]). Finally, PROCHECK[38] was used for checking the stereochemical quality of the protein structure. In the Supporting Information section, we report the PROCHECK results of the two homology models (see Table S2) and their Ramachandran plots (see Figure S1 and Figure S2).

Binding Site Identification. SiteMap has been used to highlight regions suitable for ligand binding. SiteMap can treat

dx.doi.org/10.1021/ci400180f | J. Chem. Inf. Model. 2013, 53, 1804–1817

Table 2. Protein Sequence Identity between human, murine, and rat mPGES-1 Computed with ClustalW Using the Web Service Align Tool Provided by UniProt[44]

entry name	protein names	organism	length	identity	Score	*E* value	3D
PTGES_HUMAN	mPGES-1	*Homo sapiens*	152	100	311	1.00×10^{-83}	2D crystals
Q5I0P8_RAT	mPGES-1	*Rattus norvegicus*	152	81	245	9.00×10^{-64}	
PTGES_MOUSE	mPGES-1	*Mus musculus*	153	79	244	3.00×10^{-63}	

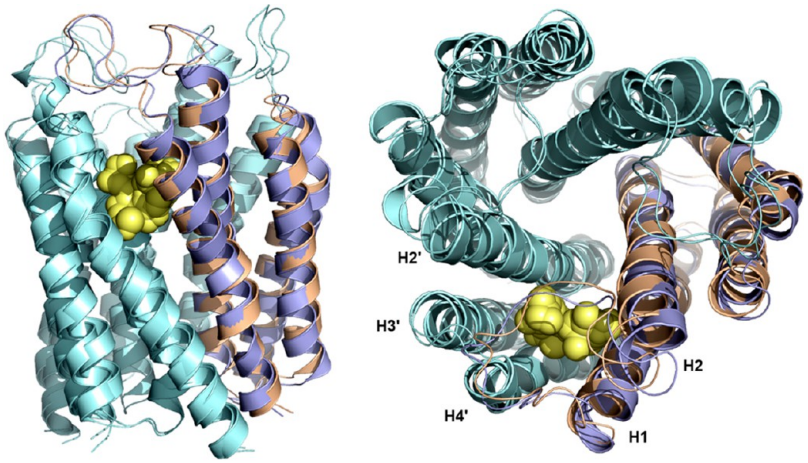

Figure 4. Superimposition between murine HM1 homology model (wheat colored ribbons) and human mPGES-1 structure (PDB: 3DWW, violet colored ribbons): front view (left) and section view (right), GSH being yellow colored (only one binding site and one monomer is highlighted for clarity).

entire proteins to locate binding sites whose size, functionality, and extent of solvent exposure meet user specifications. SiteScore, the scoring function used to assess a site's propensity for ligand binding, accurately ranks possible binding sites to eliminate those likely not to be pharmaceutically relevant. Using the standard definition of hydrophobicity and the default force field, at least of 15 site points have been requested as site dimensions.

Docking and Induced Fit Docking. Glide[39] was used for standard precision SP flexible docking of GSH and of active compounds into the built homology models; no hydrogen constraint was set, and standard protein and ligand van der Waals scaling were used (1.0 and 0.8, respectively). Enrichment factors were computed according to the formula in eq 1.[40] Aimed to take into account the protein flexibility upon ligand binding (also referred to as "induced fit" effect), we used the Schrödinger induced-fit docking protocol,[41] without any mutation into alanine prior to the first docking step.

Ligand and Protein Preparation. The ligand 2D structures were converted into 3D with LigPrep,[42] using the PRCG energy method, the OPLS_2005 all-atom force field for ligands as well as for cofactors, and treating solvation energies and effects via the SGB continuum solvation model. The protein 3D structures were prepared with the Schrödinger Protein Preparation Wizard,[36] which generates an all atom structure, filling in missing loops and side chains, optimizes H-bond network and cocrystallized ligands as well as ionizable residues protonation states, and minimizes the overall structure.

$$EF = (Hits_{sampled}/Hits_{total})(N_{sampled}/N_{total}) \quad (1)$$

Pharmacology. Starting from the native mouse PTGES constructs, four mouse mutant mPGES-1 proteins (R39A, R125A, R127A, and a double mutant R39A/R125A) were generated and expressed in *E. coli*. The protein expression was evaluated by western blotting, and the bacterial membrane preparations were used to perform the enzymatic assay. The enzyme activity was assessed quantifying the PGE_2 production with the ELISA method. The methodological details are reported in the Supporting Information.

RESULTS AND DISCUSSION

To drive the active identification efforts toward concurrent human and murine inhibitors and to gain insight of the active site of the enzyme, we provide both closed and open murine mPGES-1 3D models. For this purpose, protein homology modeling and site-directed mutagenesis, validated by means of enzymatic studies, have been combined. A comparison of the amino acid sequences between human and murine mPGES-1 reveals 79% sequence identity (see Table 2), suggesting a conserved common fold. Since 79% sequence identity is a very good value for homology modeling, the recently released[19] human coordinates of mPGES-1, describing an *apo* conformation of the enzyme, were used as a template to build the first murine homology model (named HM1 in the present work). With the aim of devising an open conformation of the murine enzyme, the human LTC_4S 3D structure was chosen as a template to build the second homology model (named HM2 in the present work). As detailed below, the MAPEG member LTC_4S, although with a low sequence homology of 16%, shares with mPGES-1 the overall trimeric structure and many catalytic residues, making it a suitable template for our purposes.

Closed Conformation of Murine mPGES-1. The 3D homology model of murine mPGES-1 in its closed conformation was built using the coordinates from the recently reported crystal structure of the human mPGES-1 (PDB code 3DWW)[19] and adding the cofactor GSH in the building step. The three monomers were built repeating the building step (ignoring any symmetry) three times, and they were then merged together to obtain the overall trimer, which is only slightly different from the template, as confirmed by the small

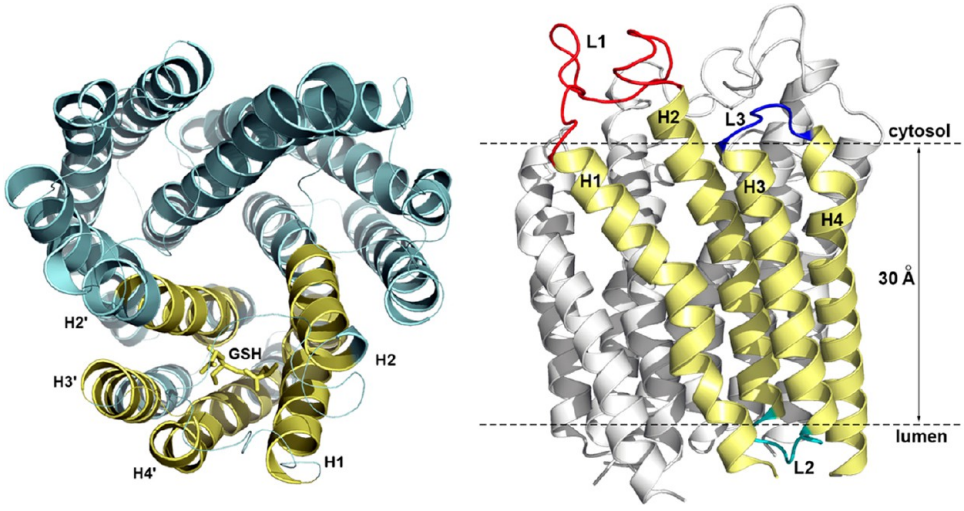

Figure 5. HM1 homology model, ribbons view: highlight of one GSH binding site (left) and highlight of one single monomer (right), with the three loops differently colored (red, blue, and cyan).

RMSD value of 1.1 Å (all-atom protein structure alignment), as illustrated in Figure 4, where the homology model indicated as HM1 was superimposed onto the human mPGES-1 3D structure. The GSH binding site is located at the interface between neighboring monomers (see Figures 4 and 5, GSH being yellow colored), and PGH_2 is supposed to bind close to GSH.[19,22] Each monomer (highlighted in Figure 5) is composed of four transmembrane helices (H1−H4) spanning residues 10−40, 60−90, 96−120, and 124−151 (mouse mPGES-1 numbering). Each of the three binding sites is located between H1, H2, H2′, H3′, and H4′ (neighboring monomers). Model quality was checked by the Ramachandran plots and PROCHECK analyses, indicating that most of the residues are in the favored regions: 85.6% most favored, 11.7% allowed, and all the critical points away from the suggested binding site (see Table S2 and Figure S1 in the Supporting Information). Three loops connect the helices: L1 (res. 41−59), L2 (res. 91−95), and L3 (res. 121−123) (see Figure 5). L1 is oriented toward the interior of the membrane. It is very long and highly flexible; hence its conformation could be very important for the enzyme functionality. The second loop (L2) is quite short (res. 91−95), and it is oriented toward the exterior of the membrane, likely facing the COXs enzymes, which provide the endogen substrate PGH_2.[19,22] Finally, the shortest loop L3 is oriented toward the exterior of the membrane. The HM1 model was used to determine the main differences between the human and the murine enzymes. Analysis of the GSH binding site indicates the murine binding site to be smaller than the human one, the volume surfaces being 863.4 $Å^3$ and 885.2 $Å^3$, respectively (see Figure 6). The different dimensions are determined by either sequence differences between the two enzymes or different orientations of identical residues. In Figure 7, the GSH binding sites of murine and human 3D structures are illustrated, showing that in the murine structure some of the residues either are more directed toward the GSH than in the human site (light green colored residues in Figure 7, right) or determine more steric hindrance (orange colored residues and orange surfaces in Figure 7, left and right). In particular, the residue-by-residue comparison shows that several sequence differences are present in the 10 Å box from the GSH (orange colored residues in Figure 7, right), causing a consistent steric hindrance if

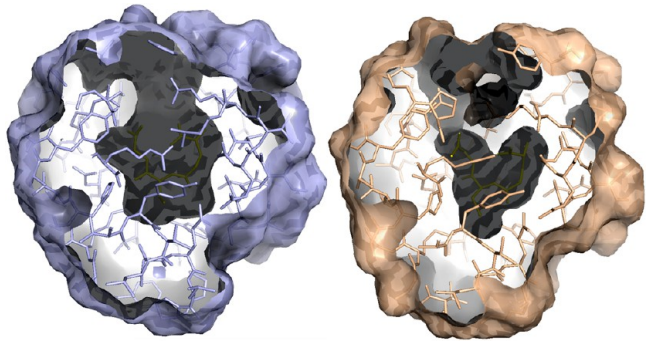

Figure 6. GSH binding surfaces of human mPGES-1 structure (PDB: 3DWW, light blue colored) and murine HM1 homology model (wheat colored). Boxes of 10 Å from GSH molecules are shown; GSH binding site surfaces illustrated as dark surfaces, and protein residues represented as sticks.

compared to the human 3D structure. In Figure 8, the human and murine mPGES-1 sequence alignment is reported, highlighting the sequence differences (yellow filled), highlighting the kind of difference: conserved residues (blue colored box), semiconserved residues (green colored box), and nonconserved residues (red colored box). In the same figure, the residues important for the functional activity of the enzyme are also illustrated (light blue filled). In detail (see Figure 7, right), in the upper region of the GSH binding site, the murine mPGES-1 P124 and R125 residues (A123 and P124 in the human enzyme) are directed toward GSH, causing a reduction in the murine binding site dimension. The different orientations of R74/R73 residues (murine/human numbering, respectively) determine a closure in the murine binding site back to the GSH. Y131 is 90° bent if compared to the human Y130 in 3DWW (see Figure 7, right), and it is involved in π-cation interaction with R127, which in turn coordinates the two GSH carboxylate functions. The orientations of Y131 and R127 also contribute to the smaller dimension of the murine mPGES-1 GSH binding site. Three sequence differences are also located at the bottom of the binding site, that is L135/F136, P136/S137, and A138/F139 (murine/human numbering, respectively), illustrated on the right in Figure 7. These residues are quite distant from GSH in the closed enzyme conformation

dx.doi.org/10.1021/ci400180f | J. Chem. Inf. Model. 2013, 53, 1804−1817

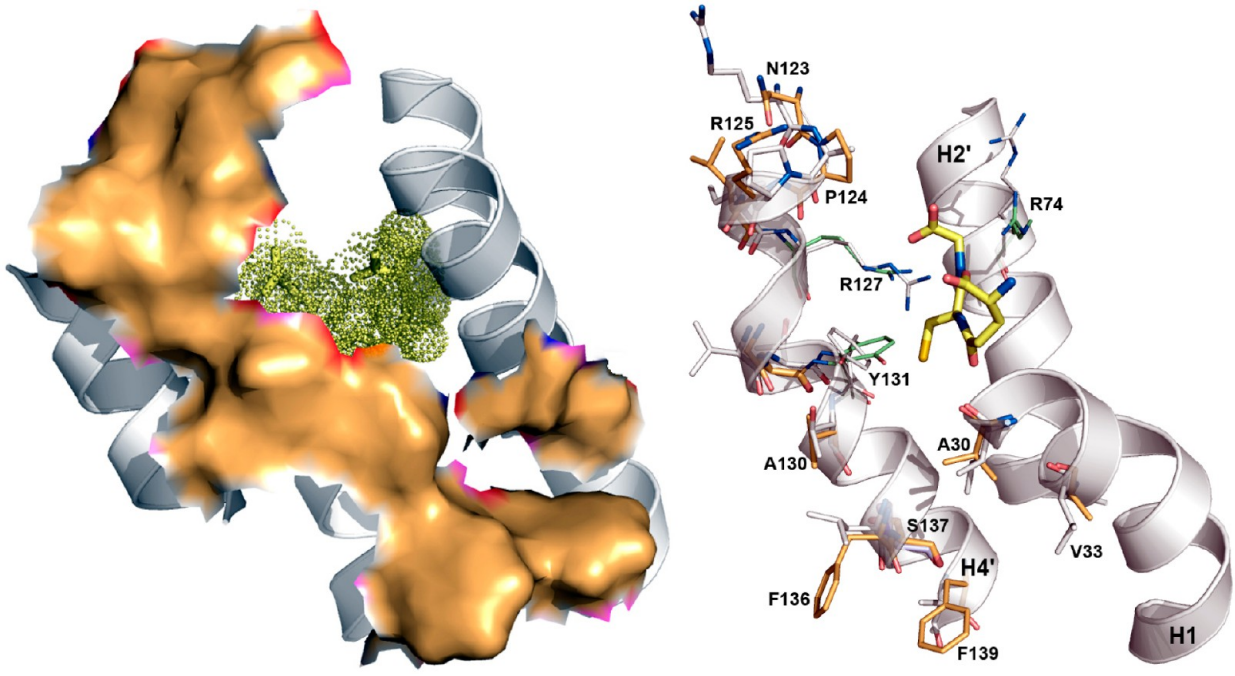

Figure 7. (Left) Front view of GSH binding site in the murine enzyme (GSH yellow colored). (Right) superimposition of human (PDB: 3DWW) and murine (HM1) GSH binding sites (GSH only from the latter 3D structure, yellow colored): the human residues are white colored; the murine residues are either light orange (sequence differences) or light green colored (different orientations). For simplicity, only the ribbons and residue numbers from the murine structure are illustrated.

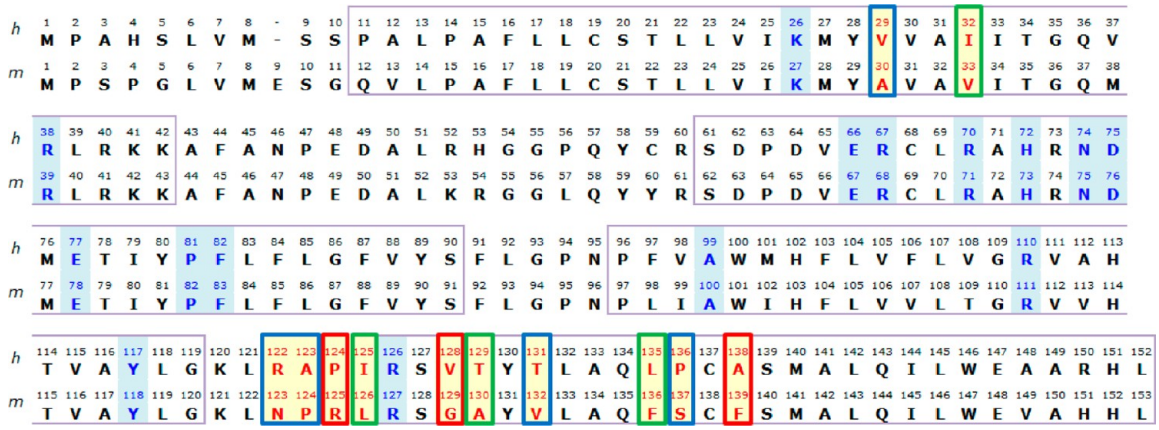

Figure 8. Sequence alignment between human and murine amino acid sequences. Identical residues, hypothesized to be important for the enzymatic activity, are light blue colored, and different residues are yellow colored (conserved, semiconserved, and not conserved residues are green-boxed, blue boxed, and red boxed, respectively). Transmembrane helix residues are boxed.

(about 10 Å), but they could be important for PGH_2 binding, as PGH_2 is hypothesized to bind in this region.[19,22] The other sequence differences (A30/V29, V33/I32, N123/R122, L126/I125, G129/V128, A130/T129, V132/T131) are mainly directed toward the exterior of the protein, but they could determine a different charge distribution in the substrate binding site, which could be relevant especially for the open/active conformation of the enzyme. Pawelzik and co-workers reported the rat enzyme GSH binding site to be smaller than the corresponding human one,[29] confirming our hypothesis about the rodent binding site dimension. The sequence difference A138/F139 was also cited in the paper,[29] but none of the residues identified in the upper region of the site had been previously described for the rodent enzyme.

Open Conformation of Murine mPGES-1: HM2. The amino acid sequence alignment revealed ∼15% identity and ∼30% homology between murine mPGES-1 and the human LTC_4S template (Table 2). Both the MAPEG members mPGES-1 and LTC_4S share the overall trimeric structure and the GSH function; the substrate binding site in the LTC4S structure is hypothesized to be localized into neighboring subunits and in mPGES-1 PGH_2 is predicted to bind in the analogues region.[19,22] All these aspects led us to select the human LTC_4S as a template for the building of the HM2 homology model, aimed to obtain the enzyme model in its open conformation. The overall trimer was obtained by merging the three monomers built separately (GSH being added in the building step), and side-chain prediction, minimization, and loop refinement gave a reliable 3D structure

dx.doi.org/10.1021/ci400180f | J. Chem. Inf. Model. 2013, 53, 1804−1817

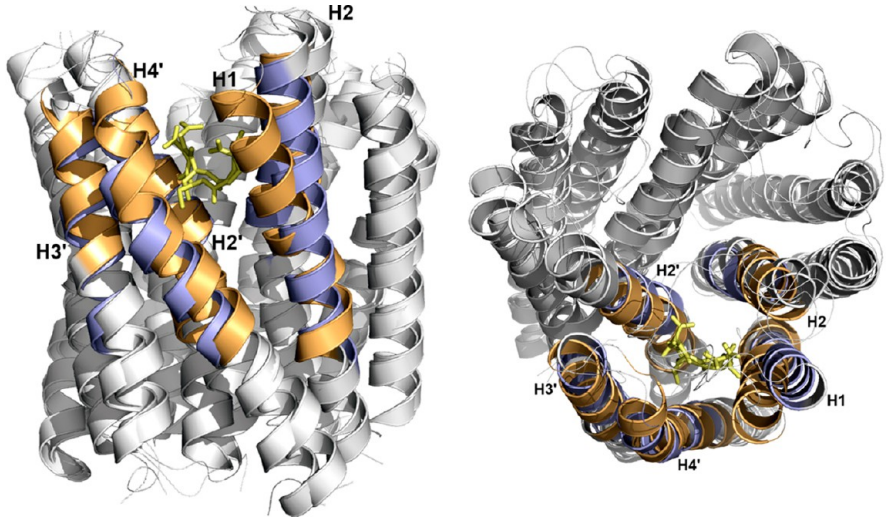

Figure 9. Superimposition of HM1 (light orange colored) and HM2 (light blue colored) models: (left) front view and (right) top view. For simplicity, only one GSH binding site is highlighted, GSH molecules being yellow colored.

conformation, as also confirmed by the Ramachandran plots and the PROCHECK analyses (85.4% of the residues being in the most favored regions, and 11.1% being in additionally allowed regions). All the critical points (less than 4%) are away from the predicted binding site (see Figure S2 and Table S2 in the Supporting Information). Other technical parameters, such as main-chain hydrogen bonding energy, bad nonbonded interactions, and peptide planarity, were also evaluated. The overall G-factor value equal to −0.23 (smaller than the G-factor equal to −0.45 of the human mPGES-1 3D structure) revealed a very good quality of the open murine mPGES-1 homology model. The superimposition between HM1 and HM2 homology models is illustrated in Figure 9, and it indicates H1 being bent in the latter model (as illustrated by the movement of Y29 and R39 residues highlighted in Figure 10), confirming an opening of the predicted binding site region,

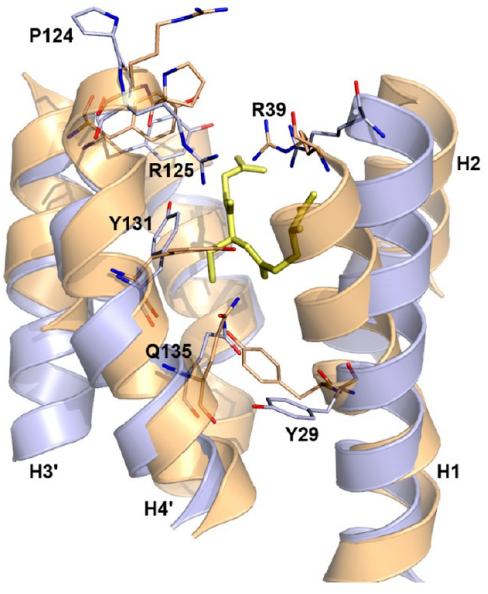

Figure 10. Superimposition of HM1 (light orange colored) and HM2 (light blue colored) GSH binding sites highlighting the different residues' orientations.

which is necessary for the catalytic activity of the enzyme.[19] The L1 loop (residues 41−60) is quite shorter in the LTC_4S than in mPGES-1; thus, for its building, we used the HM1 homology model as a template. Because of the bending of H1, loop refinement of residues 41−60 gave different conformations, which is consistent with the high L1 flexibility; the lowest energy conformation was selected for the following studies. Regarding the H2 helix, a little shift in the HM2 model is present (see Figure 9, right), contributing to restricting the mPGES-1 central cavity, which the endogen substrate should pass through. H3 and H4 helices conformations do not vary consistently compared to the HM1 model, with the exception of the Y131 residue, which is flipped in HM2 (see Figure 10). Several residues from the L3 loop, which should face the predicted substrate binding site, have different orientations (see upper left region of the binding site in Figure 10), leading the residues to come into closer contact with the L1 residues, further determining an opening of the predicted binding site. Inspection of the surface of the HM2 trimer exhibited the presence of a hole located at the interface between two neighboring monomers (see Figure 11). The GSH molecule fitted into the cavity of the trimer, bound in a U-shaped conformation. The GSH-Cys sulfur atom is hypothesized to be negatively charged, and responsible for nucleophilic attack to the PGH_2-O9 atom, necessary for the PGH_2 isomerization to PGE_2.[58] One or more arginine residues are thought to assist the reaction by the stabilization of the GSH-Cys thiolate anion and PGH_2-C9-H removal during isomerization.[19,45] Human mPGES-1 R110A mutation completely abolishes the enzyme activity,[19] and either R126A or R126Q mutations partially abolish the enzymatic activity.[45] Nevertheless, it is still not clear which is the arginine residue involved in the catalytic PGH_2 isomerization. Many arginine residues are present in the 10 Å box from GSH, and in the HM2 model the distance between the GSH sulfur atom (which likely is present as thiolate anion) and the positively charged R111 is about 2 Å (see Figure 11, right), consistent with a stabilization of the thiolate negative charge. The GSH-Gly carboxylate group is coordinated by Y131, Y118, and R127, which have been demonstrated to be fundamental for the human enzyme catalytic activity by site-directed mutagenesis experiments.[19,45,46] The GSH-Glu car-

dx.doi.org/10.1021/ci400180f | J. Chem. Inf. Model. 2013, 53, 1804−1817

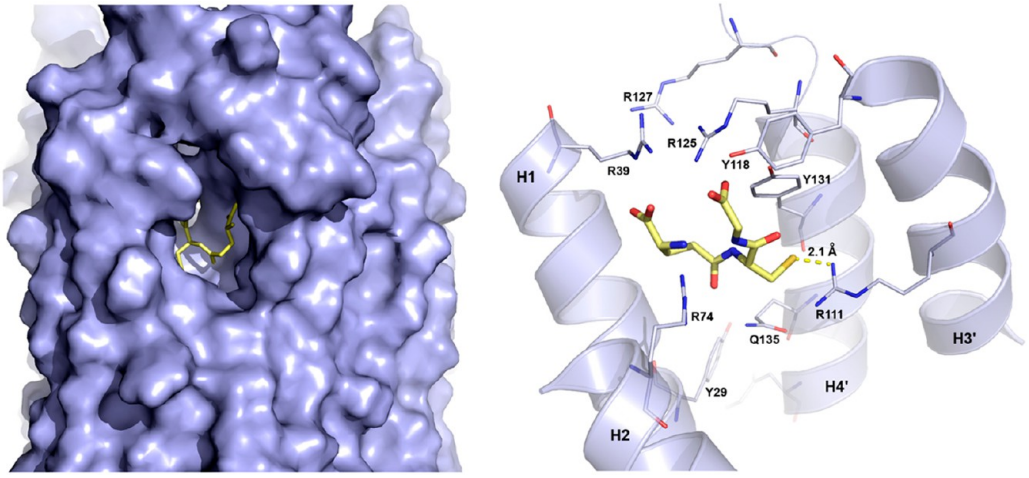

Figure 11. HM2 homology model: (left) hole near the GSH binding site (GSH being yellow colored) and (right) GSH-binding residues.

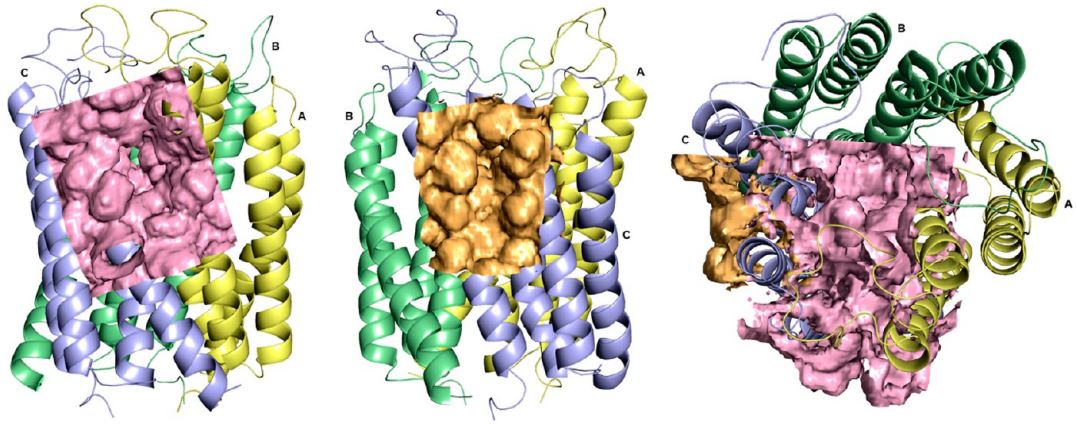

Figure 12. SiteMap results: (left) GSH binding site into HM2 homology model, (center) the predicted inter helices binding site, and (right) superimposition between the two sites.

bonyl group is coordinated by Q135, and its carboxyl groups is hydrogen bonded to the positively charged R39 residue.

To perform docking studies of a ligand into mPGES-1, a mechanism of action has been elucidated. The exact binding site localization, of course, highly influences docking results, requiring a systematic analysis of the entire protein region. GSH should be present before PGH_2 enters the binding site, which should be located near the GSH binding site, between H1 and H4′ (helix from the neighboring monomer) toward the exterior of the enzyme.[19] A few years ago, a suggested open conformation of the human enzyme was described by Hamza et al.,[47] and the binding modes of PGH_2 and GSH into the protein were generated. Exhaustively exploring protein regions other than the predicted substrate binding site could be too computationally expensive and time-consuming without any experimental data. Possible and suitable binding sites for substrate and/or inhibitor binding in the homology model were located, explored, and analyzed by means of adequate tools such as SiteMap.[48] As expected, the GSH binding site is predicted as a very likely druggable binding site in the HM2 model. It is about 560 $Å^3$ in volume, and its SiteScore is 1.09 (Figure 12). SiteMap also predicted a binding pocket in helices of a single monomer (see Figure 12, right), but its dimension prevented good fitting of inhibitors. It is interesting to compare our 3D homology model of murine mPGES-1 with the human crystal structure, deeply analyzing the differences in the GSH/PGH_2 binding site (10 Å region from GSH). As discussed above, there are 12 different residues, which can be subdivided into three groups (see Figure 8): conserved residues (green boxed), semiconserved residues (blue boxed), and not-conserved residues (red boxed). If the mPGES-1 inhibitor binding site was localized in the nonconserved region, we should expect different activity against the human and murine enzymes. Since most of the known human mPGES-1 inhibitors have no effect on the murine enzyme, this region was selected as the most likely inhibitor binding site. A conservative strategy was proposed regarding the inhibitors' mechanism of action, suggesting the active compounds to bind the murine protein in its "open/active" conformation, fitting into the substrate binding site or the region close to it. This approximation is justified by the total absence of experimental data regarding the binding site localization of the active compounds.

We also considered both the presence and the absence of the cofactor GSH. Accordingly, active compounds could displace the endogenous substrate occupying its binding site with or without GSH (the latter case could represent the situation where GSH moves from the "reactive" pose to a different one which does not influence ligands activity). Alternatively, if the ligands bound the protein close to the PGH_2 binding site, they would prevent both PGH_2 and GSH to efficiently bind the enzyme, and GSH should move from its "active" pose either

dx.doi.org/10.1021/ci400180f | J. Chem. Inf. Model. 2013, 53, 1804−1817

occupying or not a close region, justifying docking with or without GSH.

Binding of mPGES-1 with Inhibitors. The modeled 3D structure of the murine mPGES-1 trimer was used to study how the identified inhibitors bind the enzyme, and Glide software[39] was used for docking the collection of murine active compounds into the model. The predicted PGH_2 binding site, which should be located near the GSH binding site toward the exterior of the enzyme,[19,47] includes almost all the sequence differences reported in Figure 8. In the first effort, docking studies failed to predict the binding poses either with or without GSH, confirming the murine GSH binding site to be too small to accommodate ligands other than GSH, if compared to human 3D structure. Most of the murine active compounds are quite smaller than the human active compounds reported in the literature, demonstrating that nothing can be present other than GSH if the protein is kept rigid. As a consequence, failures in predicting protein ligand interactions in the murine mPGES-1 model may be attributed to the small pocket dimensions. To further account for the binding site flexibility, binding modes of active compounds were regenerated through Glide/Induced Fit Docking (IFD)[41] runs. We did not remove any residues for the initial docking step in the IFD protocol, which can then be considered as a protein relaxation in the presence of the ligand. IFD of the murine active compounds into this region generated a protein cleft which reasonably could accommodate a ligand (in Figure 13, the IFD pose of compound **1** is illustrated with the corresponding binding molecular surface, GSH being orange colored and compound **1** being green carbon colored). According to this binding mode, compound **1** inhibition will be competitive with the PGH_2 substrate. The best IFD poses of compound **1** into HM2 in terms of GScore, IFD Score, overall geometry, and overall protein interacting residues represented were further analyzed (see Figure 14). Surprisingly, docking results with and without GSH were very similar (illustrated in Figure 14), demonstrating that the small dimensions of the predicted murine binding site prevent the ligand from entering deeply into the protein also when GSH is not present. Furthermore, residues Y29, R39, Y131, and Q135 possess high flexibility, as indicated by the opposite orientations among the results. Induced-fit docking of compound **1** without GSH reveals only two ligand pose clusters (named HMm and HMm-a in the present work), mainly differing for the orientations of the above-mentioned residues Y131, Y29, Q135, and R39 (see Figure 14, center and right). In particular, if compared to HM2 with GSH (in Figure 14, left), the Y131 side chain is either 90° rotated (into HMm, in Figure 14, center) or 180° flipped (into HMm-a, in Figure 14, right); Y29 and Q135, respectively, are 90° and 180° flipped into HMm, while adopting similar conformations into HMm-a. On the contrary, R39 is 90° rotated only into HMm-a. The two binding modes HMm and HMm-a are very similar to each other, with the ligand positioned at the interface between two neighboring monomers, involving almost identical receptor residues (the receptor−ligand interactions for the two binding modes are illustrated in Figure 15). In the HMm pose (in Figure 15, left), the ligand fits into the pocket by establishing strong electrostatic interactions with Y131, R39, and R127, trapping the inhibitor carboxyl moiety into a hydrogen bond network. Furthermore, a π-cation interaction is present between the inhibitor *p*-chlorobenzyl group and R39. The ligand indole ring is stabilized in the pocket by hydrophobic interactions with V132, V33, and A32. Finally, the ligand biphenyl moiety contacts the side chains of Y29, A30, and F139, and it is directed toward the exterior of the protein. In the HMm-a pose (in Figure 15, right), the side chains of Y131, Q135, Y29, and R39 are 180° flipped, inducing the ligand to change from the pseudovertical pose (in the HMm binding mode) to the pseudohorizontal one, although establishing similar interactions. In particular, the carboxyl group of the compound is part of a complex hydrogen bond network involving R39, R125, and R127 residues, which consistently stabilize the carboxyl negative charge. Both hydrophobic and polar interactions stabilize the ligand *p*-chlorobenzyl group involving, respectively, V132 and S128/H73. Since the above-mentioned residues could be crucial for accommodating the ligands, the enrichments of both the HMm and HMm-a docking models were evaluated. These three IFD poses of compound **1** (one with GSH, two without GSH) were used to compute the docking grids and carry out docking of all the weak micromolar murine active compounds. In Figure 16, the docking poses of compound **4** and compound **5** into HMm are illustrated. Results showed for almost all active compounds common interactions with three arginine residues, which are named "the catalytic triad" in the present work: R125 (P124 in the human enzyme), R127, and R39. Hydrogen bond interactions with S127 have often been detected, as in the case of compound **5** (see Figure 16, right), as well as polar interactions with Q135 (see Figure 16, left). Many hydrophobic interactions also contribute to the ligand stabilization, involving A32, V33, V132, and the aromatic residues Y131, F136, Y29, and F139, the latter two especially contacted by the biggest active compounds. These aromatic residues were thus hypothesized to be important in coordinating the ligand hydrophobic end, but not fundamental for the catalytic activity. To quantify the murine mPGES-1 model's ability to assign high ranks to ligands with known binding affinity, we report enrichment factors in graphical form and present accumulation curves that show how the fraction of recovered actives varies with the percent of the screened database. As database ligands, we employed "druglike" decoy molecules,[39] averaging 400 Da in molecular weight in most cases, and seven weak active compounds (MK886 and

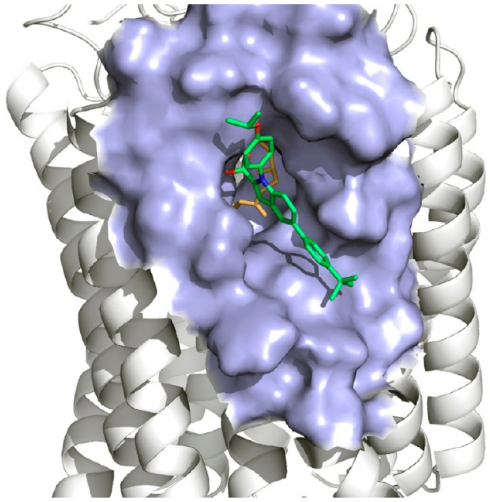

Figure 13. Binding surface of one IFD pose of compound **2** into the HM2 homology model (compound **2**, green carbon colored; GSH, orange colored).

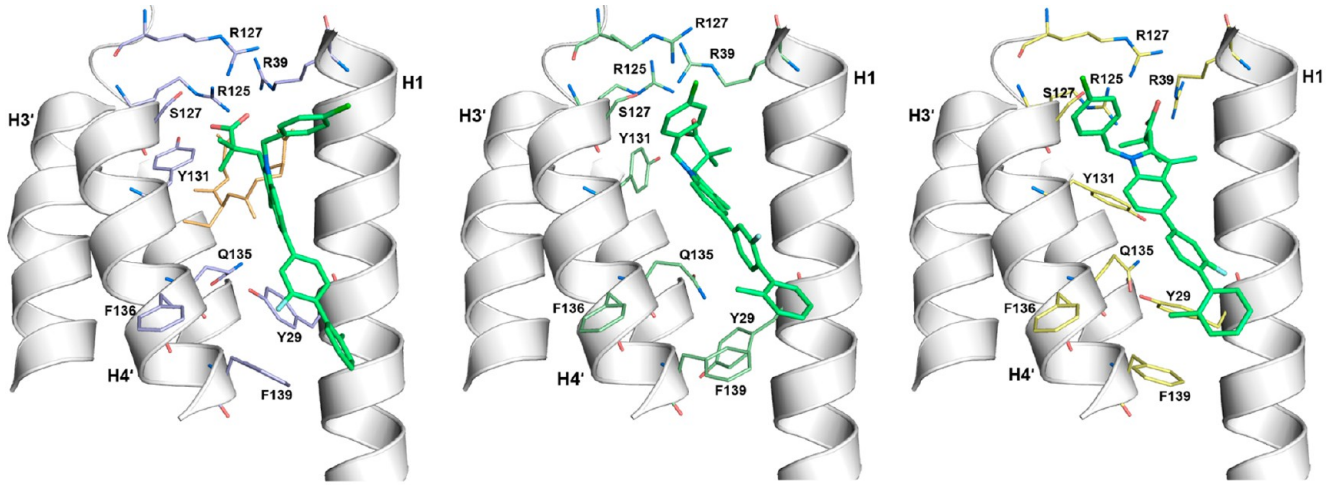

Figure 14. IFD pose of compound **1** into the HM2 model with GSH (left) and two IFD poses of **1** into HM2 without GSH (HMm, center; HMm-a, right). Ligands are green carbon colored, and GSH is orange colored.

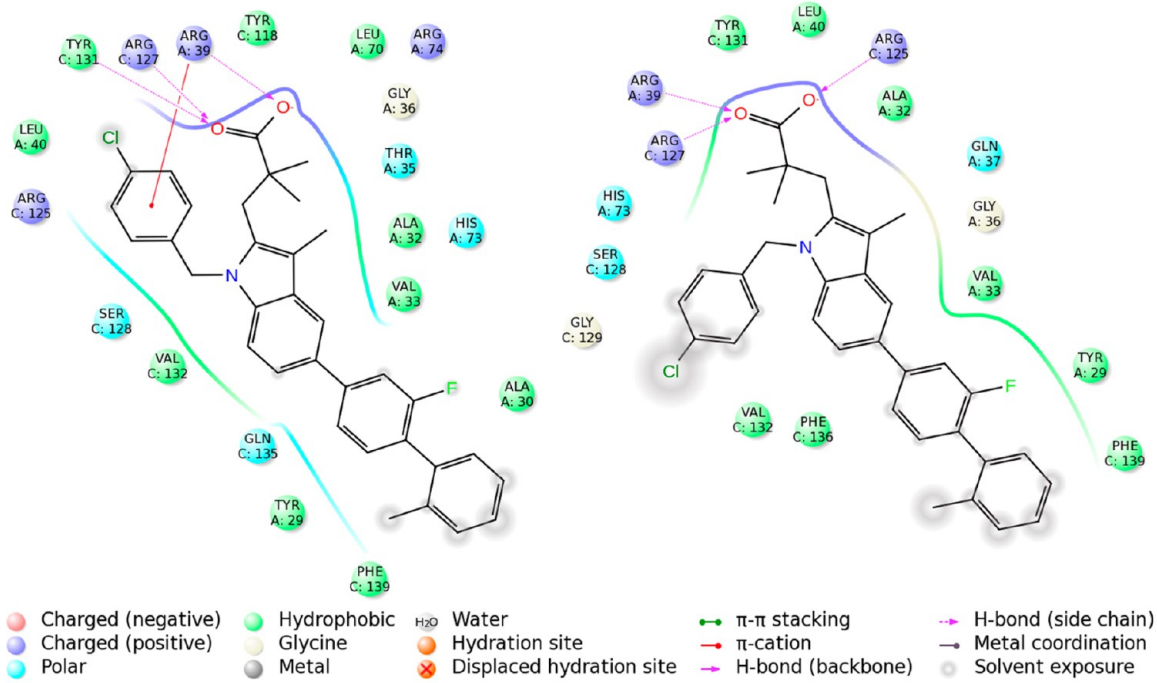

Figure 15. Receptor–ligand interactions for the first binding mode (HMm, left) and the second binding pose (HMm-a, right) of compound **1** into the HM2 model without GSH.

compounds **1**–**6**). Docking into HM2 with GSH indicated that the docking model is able to retrieve active compounds, even if its performance can be refined (the enrichment factor EF graph is illustrated in Figure 17). For the two models without GSH, docking of the test set into both HMm and HMm-a performed even better (see Figure 18 for the EF graphs, left and right, respectively). Ensemble docking of HMm and HMm-a models did not improve the results, because of different GScore values between the two docking models (higher negative values for HMm). Given that only seven compounds were shown to moderately inhibit the murine mPGES-1, the performances of all the generated docking models are not as good as one might expect. The binding modes with or without GSH are very close, and the corresponding enrichments do not vary consistently. Conversely, as mentioned above, the two models without GSH show some differences in the binding site, owing to the opposite side chain conformations of Y29, R39, Y131, and Q135 residues. Aimed at taking into account the protein flexibility, both the docking models without GSH were selected for virtual screening of corporate and commercial libraries to identify new murine hit compounds (manuscript in preparation).

***In Silico* Guided Site-Directed Mutagenesis Experiments.** In light of these earlier results, we investigated the protein residues' mutations to elucidate the binding mode of inhibitors in the mPGES-1 trimer. In the literature, many mutagenesis experiments were performed on the human enzyme,[19,45−47] but no data on the murine enzyme are reported. As a consequence and due to high sequence identity and sequence homology between human and murine mPGES-1, the available mutagenesis data of the human protein were considered, assuming the residues predicted fundamental for

dx.doi.org/10.1021/ci400180f | J. Chem. Inf. Model. 2013, 53, 1804−1817

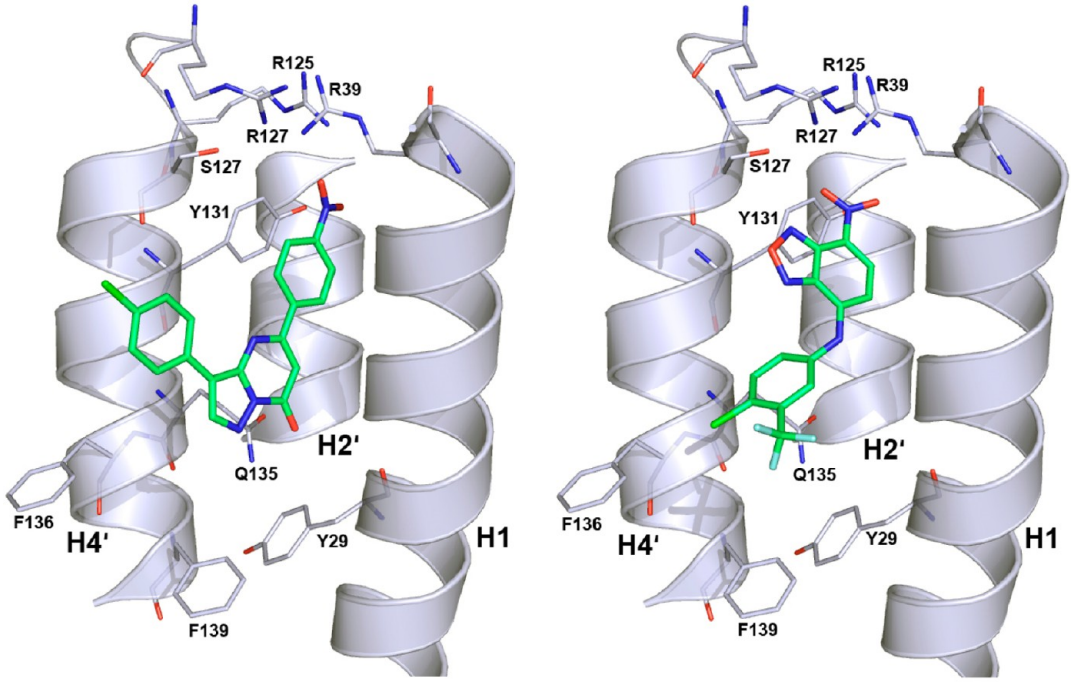

Figure 16. Docking pose of compounds **4** (left) and **5** (right) into the HMm-a model. Ligands are green carbon colored, and interacting residues are white-blue colored.

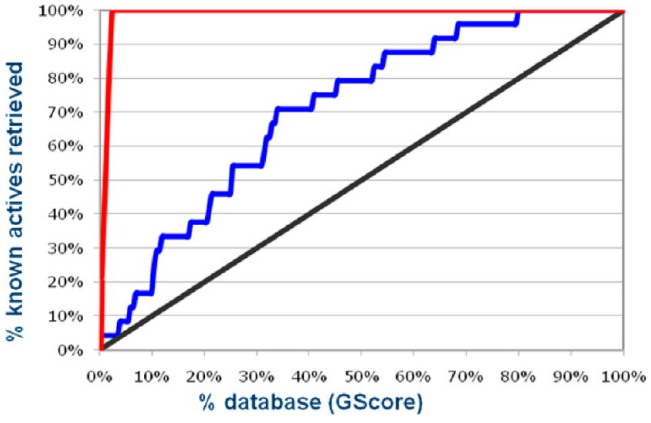

Figure 17. Enrichment factor graph for docking of the test set into HM2 with GSH.

enzymatic activity to be conserved among the two species. Table 3 shows the mutation influence on human enzyme activity[19,46,47] for each residue (the color scale is reported at the end of the Table 3). Mutation of some residues completely abolishes enzymatic activity, indicating that they are fundamental for the enzyme to catalyze PGH_2 isomerization. Considering a single residue, for a docking binding mode to be validated by mutagenesis, an active compound should not inhibit mutated enzymes if interacting with the given residue. If a given residue mutation partially or completely abolished enzyme activity, docking binding mode validation involving that residue could not be possible since inhibitor activity could not be measured. Our protein-based murine mPGES-1 modeling approach was used to design site-directed mutagenesis studies to elucidate the main differences between the human and the murine enzyme and to determine the binding mode of identified weak murine active compounds. The docking models

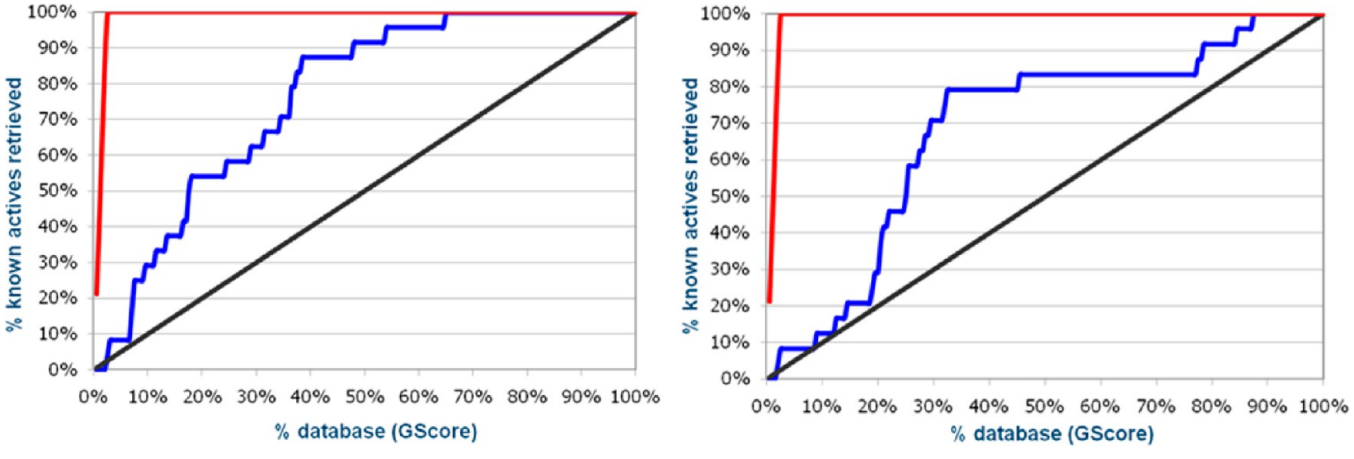

Figure 18. Enrichment factor graphs for docking of the test set into HMm (left) and HMm-a (right).

dx.doi.org/10.1021/ci400180f | J. Chem. Inf. Model. 2013, 53, 1804−1817

Table 3. Literature Available Mutagenesis Data on Human mPGSE-1[a]

Abolished	10-20%	20-30%	30-40%	40-60%	60-80%	Full
R67A	Y130I	R110T	H72A	Q134E	R70A	R70S
E77A	R126A	T114V			Q36E	Y117F
R110A	N74A				E66A	R122A
Y117A	T129V					

[a]Residues are colored according to the detected enzyme activity after mutation (the scale is reported in the top row).

suggested nine residues to be important for the ligands' activity: R127, R125, R39, Y131, S128, Y29, F139, V33, and V132. F139 was recently denoted important for the rat enzyme,[29] and R127 and Y131 are shown to be fundamental for human enzyme catalytic activity. The arginine residues of the catalytic "triad" were mutated into alanine (R39A, R125A, and R127A). In the case of partial activity of the R39A and R125A mutants, the double mutation R39A/R125A could demonstrate the need for the presence of at least two of the three arginine residues for the catalytic activity. The PGE_2 production of the four mutants and the WT enzyme are reported in Table S4, and the corresponding curves are illustrated in Figure 19. All the

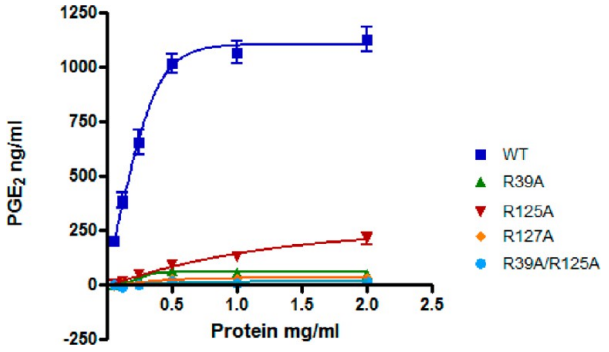

Figure 19. Mutagenesis experiments of murine mPGES-1: graph of the PGE_2 production of R39A, R125A, R127A, and R39A/R125A mutants compared to WT enzyme.

mutants showed very small or absent PGE_2 production compared to the WT enzyme. Mutagenesis experiments confirmed the importance of the conserved residue R127 for the catalytic activity of the murine enzyme (R126 in the human enzyme). Furthermore, R39 and R125 were also shown to be fundamental for the activity, and notably R125 is a proline in the human enzyme. The *in vitro* inhibition assays of active compounds against the mutants could not be performed for the loss of activity of the enzymes.

CONCLUSION

Computational simulations based on our developed model of murine mPGES-1 trimer structure, followed by site-directed mutagenesis and mPGES-1 activity assay, led us to a better understanding of how the mPGES-1 trimer interacts with inhibitors. The present work provides the following key insights on murine mPGES-1: (1) It identifies residues that are crucial for inhibitor interactions. (2) It elucidates the binding mode. Two homology models were built using the 3D structure of human mPGES-1 and human LTC_4S as templates, aimed at hopefully describing both the closed and the open conformations of murine mPGES-1. These models were analyzed and validated by adequate tools, such as Schrödinger Protein Reports, Ramachandran maps, and PROCHECK. The HM1 homology model (likely describing the closed enzyme conformation) was compared to the human 3D-structures, identifying some sequence differences that could explain the observed smaller *dimension* of the murine GSH binding site. Analysis of the HM2 homology model (likely describing the open enzyme conformation) indicates the 12 differences in the human/murine protein sequence to be mostly localized in the predicted substrate binding site. For some of these residues, their dimensions are quite bigger in the murine enzyme than in the human one, likely contributing to the smaller dimension of the murine predicted binding site. The available weak active compounds were suggested to bind the protein in the GSH/PGH_2 binding site in the "open/active" conformation of the enzyme, likely described by the HM2 homology model. Docking and IFD of active compounds into this region gave reasonable and conserved binding modes. In particular, ligands cannot enter deeper into the protein, probably due to the smaller dimensions of the murine predicted binding site. Active compounds were predicted by the docking model to interact mainly with three residues (R125, R127, and R39), which were thus proposed to be fundamental for activity, and named the "catalytic triad." Ionic interactions with S128 and Y131 were also detected for many of the actives. Hydrophobic interactions with Y29, V33, V132, and F139 also appeared to be important for some of the actives, even if not sufficient alone for ligand activity. Three residues were selected for the mutagenesis experiments (R39, R125, and R127), and the results indicated all of them to be fundamental for the enzyme catalytic activity. In particular, the conserved MAPEG R127A was confirmed to be necessary also for the murine enzyme. The R38A and P124A mutations (corresponding to R39A and the R125A mutations in the present work) were never reported in the literature for the human enzyme, and notably, R125 is a proline in the human protein. The predicted binding modes in HM2 can thus be considered as partially validated, and HM2 could be used for virtual screening studies aimed at identifying new murine hit compounds. Following SAR studies using the murine hits could allow the obtainment of dual human/murine mPGES-1 inhibitors. We actually performed virtual screening of corporate and commercial libraries into the selected docking models, and the results will be presented elsewhere (manuscript in preparation).

ASSOCIATED CONTENT

Supporting Information

Some homology models details and biological data, reported into text, three figures, and four tables. This material is available free of charge via the Internet at http://pubs.acs.org.

AUTHOR INFORMATION

Corresponding Author

*Phone: +39 06 91045289 (G.C.), +39 06 91045375 (R.O.). E-mail: g.corso@angelini.it (G.C.), r.ombrato@angelini.it (R.O.).

Notes

The authors declare no competing financial interest.

■ ACKNOWLEDGMENTS

We wish to thank Dr. Francesca Mancini and Marco Vitiello (In vitro Pharmacology Dev., Angelini Research Center) for their technical support. G.C. and R.O. acknowledge Dr. Elena Fioravanzo and Dr. Arianna Bassan (S-IN Soluzioni Informatiche Srl, via Ferrari 14, I-36100 Vicenza - Italy) for the helpful discussions and their kind review.

■ ABBREVIATIONS

CCR2, CC chemokine receptor 2; CCL2, CC chemokine ligand 2; CCR5, CC chemokine receptor 5; GSH, glutathione; TLC, thin layer chromatography

■ REFERENCES

(1) Jakobsson, P. J.; Thoren, S.; Morgenstern, R.; Samuelsson, B. Identification of Human Prostaglandin E Synthase: A Microsomal, Glutathione-dependent, Inducible Enzyme, Constituting a Potential Novel Drug Target. *Proc. Natl. Acad. Sci. U. S. A.* **1999**, *96*, 7220−7225.

(2) Guan, Y.; Zhang, Y.; Schneider, A.; Riendeau, D.; Mancini, J. A.; Davis, L.; Komhoff, M.; Breyer, R. M.; Breyer, M. D. Urogenital distribution of a mouse membrane-associated prostaglandin E(2) synthase. *Am. J. Physiol.: Renal, Fluid Electrolyte Physiol.* **2001**, *281*, F1173−1177.

(3) Tanikawa, N.; Ohmiya, Y.; Ohkubo, H.; Hashimoto, K.; Kangawa, K.; Kojima, M.; Ito, S.; Watanabe, K.; Kurihara, K. Identification and characterization of a novel type of membrane-associated prostaglandin E synthase. *Biochem. Biophys. Res. Commun.* **2002**, *291*, 884−889.

(4) Tanioka, T.; Nakatani, Y.; Semmyo, N.; Murakami, M.; Kudo, I. Molecular identification of cytosolic prostaglandin E2 synthase that is functionally coupled with cyclooxygenase-1 in immediate prostaglandin E2 biosynthesis. *J. Biol. Chem.* **2000**, *275*, 32775−32782.

(5) Kobayashi, T.; Narumiya, S. Function of prostanoid receptors: studies on knockout mice. *Prostaglandins Other Lipid Mediators* **2002**, *68−69*, 557−573.

(6) (a) Nakanishi, M.; Gokhale, V.; Meuillet, E. J.; Rosenberg, D. W. mPGES-1 as a target for cancer suppression: A comprehensive invited review ″Phospholipase A2 and lipid mediators. *Biochimie* **2010**, *92* (6), 660−664. (b) Samuelsson, B.; Morgenstern, R.; Jakobsson, P.-J. Membrane Prostaglandin E Synthase-1: A Novel Therapeutic Target. *Pharmacol. Rev.* **2007**, *59*, 207−224.

(7) Trebino, C. E.; Stock, J. L.; Gibbons, C. P.; Naiman, B. M.; Wachtmann, T. S.; Umland, J. P.; Pandher, K.; Lapointe, J. M.; Saha, S.; Roach, M. L.; Carter, D.; Thomas, N. A.; Durtschi, B. A.; McNeish, J. D.; Hambor, J. E.; Jakobsson, P. J.; Carty, T. J.; Perez, J. R.; Audoly, L. P. Impaired inflammatory and pain responses in mice lacking an inducible prostaglandin E synthase. *Proc. Natl. Acad. Sci. U. S. A.* **2003**, *100*, 9044−9049.

(8) Nakanishi, M.; Montrose, D. C.; Clark, P.; Nambiar, P. R.; Belinsky, G. S.; Claffey, K. P.; Xu, D.; Rosenberg, D. W. Genetic deletion of mPGES-1 suppresses intestinal tumorigenesis. *Cancer Res.* **2008**, *68*, 3251−3259.

(9) Kamei, D.; Murakami, M.; Sasaki, Y.; Nakatani, Y.; Majima, M.; Shikawa, Y.; Ishii, T.; Uematsu, S.; Akira, S.; Hara, S.; Kudo, I. Microsomal prostaglandin E synthase-1 in both cancer cells and hosts contributes to tumour growth, invasion and metastasis. *Biochem. J.* **2010**, *425*, 361−371.

(10) Grosser, T.; Fries, S.; FitzGerald, G. A. *J. Clin. Invest.* **2006**, *116*, 4−15.

(11) McAdam, B. F.; Catella-Lawson, F.; Mardini, I. A.; Kapoor, S.; Lawson, J. A.; FitzGerald, G. A. *Proc. Natl. Acad. Sci. U. S. A.* **1999**, *96*, 272−277.

(12) Patrignani, P.; Sciulli, M.; Manarini, S.; Santini, G.; Cerletti, C.; Evangelista, V. *J. Physiol. Pharmacol.* **1999**, *50*, 661−667.

(13) Chang, H.-H.; Meuillet, E. J. Identification and development of mPGES-1 inhibitors: where we are at? *Future Med. Chem.* **2011**, *3* (15), 1909−1934.

(14) (a) Molina, D. M.; Eshaghi, S.; Nordlund, P. Catalysis within the lipid bilayer - structure and mechanism of the MAPEG family of integral membrane proteins. *Curr. Opin. Struct. Biol.* **2008**, *18*, 442−449. (b) Bresell, A.; Weinander, R.; Lundqvist, G.; Raza, H.; Shimoji, M.; Sun, T.-H.; Balk, L.; Wiklund, R.; Eriksson, J.; Jansson, C.; Persson, B.; Jakobsson, P. J.; Morgenstern, R. Bioinformatic and enzymatic characterization of the MAPEG superfamily. *FEBS J.* **2005**, *272*, 1688−1703.

(15) Jakobsson, P. J.; Morgenstern, R.; Mancini, J.; Ford-Hutchinson, A.; Persson, B. Common structural features of MAPEG - a widespread superfamily of membrane associated proteins with highly divergent functions in eicosanoid and glutathione metabolism. *Protein Sci.* **1999**, *8* (3), 689−692.

(16) (a) Lam, B. K.; Austen, K. F. Leukotriene C4 synthase: a pivotal enzyme in cellular biosynthesis of the cysteinyl leukotrienes. *Prostaglandins Other Lipid Mediators* **2002**, *68−69*, 511−520. (b) Bisgaard, H. Leukotriene Modifiers in Pediatric Asthma Management. *Pediatrics* **2001**, *107* (2), 381−390.

(17) Byrum, R. S.; Goulet, J. L.; Griffiths, R. J.; Koller, B. H. Role of the 5-Lipoxygenase−activating Protein (FLAP) in Murine Acute Inflammatory Responses. *J. Exp. Med.* **1997**, *185* (6), 1065−1075.

(18) (a) Johansson, K.; Ahlen, K.; Rinaldi, R.; Sahlander, K.; Siritantikorn, A.; Morgenstern, R. Microsomal glutathione transferase 1 in anticancer drug resistance. *Carcinogenesis* **2007**, *28* (2), 465−470. (b) Siritantikorn, A.; Johansson, K.; Ahlen, K.; Rinaldi, R.; Suthiphongchai, T.; Wilairat, P.; Morgenstern, R. Protection of cells from oxidative stress by microsomal glutathione transferase 1. *Biochem. Biophys. Res. Commun.* **2007**, *355*, 592−596. (c) Holm, P. J.; Bhakat, P.; Jegerschöld, C.; Gyobu, N.; Mitsuoka, K.; Fujiyoshi, Y.; Morgenstern, R.; Hebert, H. Structural Basis for Detoxification and Oxidative Stress Protection in Membranes. *J. Mol. Biol.* **2006**, *360*, 934−945. (d) Morgenstern, R.; Guthenberg, C.; Depierre, J. W. Microsomal Glutathione S-Transferase: Purification, Initial Characterization and Demonstration that It Is not Identical to the Cytosolic Glutathione S-Transferases A, B and C. *Eur. J. Biochem.* **1982**, *128*, 243−248.

(19) Jegerschöld, C.; Pawelzik, S.-C.; Purhonen, P.; Bhakat, P.; Gheorghe, K. R.; Gyobu, N.; Mitsuoka, K.; Morgenstern, R.; Jakobsson, P.-J.; Hebert, H. Structural basis for induced formation of the inflammatory mediator prostaglandin E2. *Proc. Natl. Acad. Sci. U. S. A.* **2008**, *105*, 11110−11115.

(20) Busenlehner, L. S.; Codreanu, S. G.; Holm, P. J.; Bhakat, P.; Hebert, H.; Morgenstern, R.; Armstrong, R. N. Stress Sensor Triggers Conformational Response of the Integral Membrane Protein Microsomal Glutathione Transferase 1. *Biochemistry* **2004**, *43*, 11145−11152.

(21) Busenlehner, L. S.; Ålander, J.; Jegerschöld, C.; Holm, P. J.; Bhakat, P.; Hebert, H.; Morgenstern, R.; Armstrong, R. N. Location of Substrate Binding Sites within the Integral Membrane Protein Microsomal Glutathione Transferase-1. *Biochemistry* **2007**, *46*, 2812−2822.

(22) (a) Ago, H.; Kanaoka, Y.; Irikura, D.; Lam, B. K.; Shimamura, T.; Austen, K. F.; Miyano, M. Crystal structure of a human membrane protein involved in cysteinyl leukotriene biosynthesis. *Nature* **2007**, *448*, 609−612. (b) Martinez Molina, D.; Wetterholm, A.; Kohl, A.; McCarthy, A. A.; Niegowski, D.; Ohlson, E.; Hammarberg, T.; Eshaghi, S.; Haeggström, J. Z.; Nordlund, P. Structural basis for synthesis of inflammatory mediators by human leukotriene C4 synthase. *Nature* **2007**, *448*, 613−616.

(23) Jegerschöld, C.; Jakobsson, P.-J.; Hebert, H. Protein Structure and method of using protein structure. WO 2009/092800 A1, NOVASAID AB; Nobels väg 3, S-171 77 Stockholm (SE).

(24) Thorén, S.; Weinander, R.; Saha, S.; Jegerschöld, C.; Pettersson, P. L.; Samuelsson, B.; Hebert, H.; Hamberg, M.; Morgenstern, R.; Jakobsson, P.-J. Human Microsomal Prostaglandin E Synthase-1

Purification, Functional Characterization, and Projection Structure Determination. *J. Biol. Chem.* **2003**, *278*, 22199−22209.
(25) Ferguson, A. D.; McKeever, B. M.; Xu, S.; Wisniewski, D.; Miller, D. K.; Yamin, T.-T.; Spencer, R. H.; Chu, L.; Ujjainwalla, F.; Cunningham, B. R.; Evans, J. F.; Becker, J. W. Crystal Structure of Inhibitor-Bound Human 5-Lipoxygenase−Activating Protein. *Science* **2007**, *317*, 510−512.
(26) Riendeau, D.; Aspiotis, R.; Ethier, D.; Gareau, Y.; Grimm, E. L.; Guay, J.; Guiral, S.; Juteau, H.; Mancini, J. A.; Méthot, N.; Rubin, J.; Friesen, R. W. Inhibitors of the inducible microsomal prostaglandin E2 synthase (mPGES-1) derived from MK-886. *Bioorg. Med. Chem. Lett.* **2005**, *15*, 3352−3355.
(27) Olofsson, K.; Suna, E.; Pelcman, B.; Ozola, V.; Katkevics, M.; Kalvins, I. Indoles Useful in the Treatment of Inflammation. WO 2005/123673 A1.
(28) Wannberg, J.; Alterman, M.; Malm, J.; Stenberg, P.; Westman, J.; Wallberg, H. WO 2011/023812 A1, NOVA-SAID AB; Fogdevreten 2A, S-17165 Solna (SE).
(29) Pawelzik, S.-C.; Uda, N. R.; Spahiu, L.; Jegerschöld, C.; Stenberg, P.; Hebert, H.; Morgenstern, R.; Jakobsson, P.-J. Identification of Key Residues Determining Species Differences in Inhibitor Binding of Microsomal Prostaglandin E Synthase-1. *J. Biol. Chem.* **2010**, *285* (38), 29254−29261.
(30) Xu, D.; Rowland, S. E.; Clark, P.; Giroux, A.; Cote, B.; Guiral, S.; Salem, M.; Ducharme, Y.; Friesen, R. W.; Methot, N.; Mancini, J.; Audoly, L.; Riendeau, D. MF63 [2-(6-chloro-1H-phenanthro[9,10-d]imidazol-2-yl)-isophthalonitrile], a selective microsomal prostaglandin E synthase-1 inhibitor, relieves pyresis and pain in preclinical models of inflammation. *J. Pharmacol. Exp. Ther.* **2008**, *326*, 754−763.
(31) (a) Maugeri, C.; Furlotti, G.; Mangano, G.; Coletta, I.; Polenzani, L.; Alisi, M. A.; Cazzolla, N. Use of a benzoyl derivative of 3-aminocarbazole for the treatment of a disorder associated with the production of prostaglandin E2 (PGE2). WO Patent WO 2006/122680, 2006. (b) Furlotti, G.; Mangano, G.; Coletta, I.; Alisi, M. A.; Cazzolla, N.; Dragone, P.; Russo, V. 3-Aminocarbazole compounds, pharmaceutical composition containing the same and method for the preparation thereof. WO Patent WO 2007/014687, 2007. (c) Maugeri, C.; Furlotti, G.; Garofalo, B.; Coletta, I.; Alisi, M. A.; Cazzolla, N.; Ombrato, R. 2-Arylindole derivatives as NPGES-I inhibitors. WO Patent WO 2008/006663, 2008. (d) Maugeri, C.; Furlotti, G.; Garofalo, B.; Coletta, I.; Alisi, M. A.; Cazzolla, N.; Dragone, P. (Aza)indole derivative substituted in position 5, pharmaceutical composition comprising it, intermediate compounds and preparation process therefor. WO Patent WO 2009/083436, 2009. (e) Guglielmotti, A.; Maugeri, C.; Furlotti, G.; Mangano, G.; Garofalo, B.; Coletta, I.; Alisi, M. A.; Cazzolla, N.; Dragone, P. 3-Aminocarbazole compound, pharmaceutical composition containing it and preparation method therefor. WO Patent WO 2009/138376, 2009.
(32) *The PyMOL Molecular Graphics System*, version 1.5.0.4; Schrödinger, LLC: New York.
(33) The UniProt Consortium. Ongoing and future developments at the Universal Protein Resource. *Nucleic Acids Res.* **2011**, *39*, D214−D219.
(34) Berman, M. H.; Westbrook, J.; Feng, Z.; Gilliland, G.; Bhat, T. N.; Weissig, H.; Shindyalov, I. N.; Bourne, P. E. The Protein Data Bank. *Nucleic Acids Res.* **2000**, *28* (1), 235−242.
(35) (a) *Prime*, version 2.1; Schrödinger, LLC: New York, 2009. (b) Jacobson, M. P.; Pincus, D. L.; Rapp, C. S.; Day, T. J. F.; Honig, B.; Shaw, D. E.; Friesner, R. A. A Hierarchical Approach to All-Atom Protein Loop Prediction. *Proteins* **2004**, *55*, 351−367. (c) Jacobson, M. P.; Friesner, R. A.; Xiang, R. A.; Honig, Z. B. On the Role of Crystal Packing Forces in Determining Protein Sidechain Conformations. *J. Mol. Biol.* **2002**, *320*, 597−608.
(36) *Schrödinger Suite 2011 Protein Preparation Wizard*; *Epik*, version 2.2; Schrödinger, LLC: New York, 2011. *Impact*, version 5.7; *Prime*, version 2.1; Schrödinger, LLC: New York, 2011.
(37) Engh, R. A.; Huber, R. Accurate bond and angle parameters for X-ray protein structure refinement. *Acta Crystallogr.* **1991**, *A47*, 392−400.
(38) Laskowski, R. A.; Macarthur, M. W.; Moss, D. S.; Thornton, J. M. PROCHECK: a program to check the stereochemical quality of protein structures. *J. Appl. Crystallogr.* **1993**, *26*, 283−291.
(39) (a) *Glide*, version 5.7; Schrödinger, LLC: New York, 2011. (b) Friesner, R. A.; Banks, J. L.; Murphy, R. B.; Halgren, T. A.; Klicic, J. J.; Mainz, D. T.; Repasky, M. P.; Knoll, E. H.; Shaw, D. E.; Shelley, M.; Perry, J. K.; Francis, P.; Shenkin, P. S. Glide: A New Approach for Rapid, Accurate Docking and Scoring. 1. Method and Assessment of Docking Accuracy. *J. Med. Chem.* **2004**, *47*, 1739−1749. (c) Halgren, T. A.; Murphy, R. B.; Friesner, R. A.; Beard, H. S.; Frye, L. L.; Pollard, W. T.; Banks, J. L. Glide: A New Approach for Rapid, Accurate Docking and Scoring. 2. Enrichment Factors in Database Screening. *J. Med. Chem.* **2004**, *47*, 1750−1759. (d) Friesner, R. A.; Murphy, R. B.; Repasky, M. P.; Frye, L. L.; Greenwood, J. R.; Halgren, T. A.; Sanschagrin, P. C.; Mainz, D. T. Extra Precision Glide: Docking and Scoring Incorporating a Model of Hydrophobic Enclosure for Protein-Ligand Complexes. *J. Med. Chem.* **2006**, *49*, 6177−6196. (e) Park, M.; Gao, C.; Stern, H. A. Estimating binding affinities by docking/scoring methods using variable protonation states. *Proteins* **2010**, *79*, 304−314.
(40) Pearlman, D. A.; Charifson, P. S. Improved scoring of ligand-protein interactions using OWFEG free energy grids. *J. Med. Chem.* **2001**, *44*, 502−511.
(41) (a) *Schrödinger Suite 2009 Induced Fit Docking protocol*; *Glide*, version 5.7; *Prime*, version 3.0; Schrödinger, LLC: New York, 2011. (b) Sherman, W.; Day, T.; Jacobson, M. P.; Friesner, R. A.; Farid, R. Novel Procedure for Modeling Ligand/Receptor Induced Fit Effects. *J. Med. Chem.* **2006**, *49*, 534−553. (c) Sherman, W.; Beard, H. S.; Farid, R. Use of an Induced Fit Receptor Structure in Virtual Screening. *Chem. Biol. Drug Des.* **2006**, *67*, 83−84. (d) Farid, R.; Day, T.; Friesner, R. A.; Pearlstein, R. A. New insights about HERG blockade obtained from protein modeling, potential energy mapping, and docking studies. *Bioorg. Med. Chem.* **2006**, *14*, 3160−3173.
(42) *LigPrep*, version 2.0; Schrödinger, LLC: New York, 2011.
(43) Schafer, P. H.; Wang, L.; Wadsworth, S. A.; Davis, J. F.; Sickierka, J. J.; Cell, T. Activation Signals Up-Regulate p38 Mitogen-Activated Protein Kinase Activity and Induce TNF-α Production in Manner Distinct from LPS Activation of Monocytes. *J. Immunol.* **1999**, *162*, 659−668.
(44) The UniProt Consortium. Reorganizing the protein space at the Universal Protein Resource (UniProt). *Nucleic Acids Res.* **2012**, *40*, D71−D75.
(45) Hammarberg, T.; Hamberg, M.; Wetterholm, A.; Hansson, H.; Samuelsson, B.; Haeggström, J. Z. Mutation of a Critical Arginine in Microsomal Prostaglandin E Synthase-1 Shifts the Isomerase Activity to a Reductase Activity That Converts Prostaglandin H2 into Prostaglandin F2α. *J. Biol. Chem.* **2009**, *284*, 301−305.
(46) Huang, X.; Yan, W.; Gao, D.; Tong, M.; Tai, H.-H.; Zhan, C.-G. Structural and functional characterization of human microsomal prostaglandin E synthase-1 by computational modeling and site-directed mutagenesis. *Bioorg. Med. Chem.* **2006**, *14* (10), 3553−3562.
(47) Hamza, A.; Tong, M.; Diwan, M.; AbdulHameed, M.; Liu, J.; Goren, A. C.; Tai, H.-H.; Zhan, C.-G. Understanding Microscopic Binding of Human Microsomal Prostaglandin E Synthase-1 (mPGES-1) Trimer with Substrate PGH_2 and Cofactor GSH: Insights from Computational Alanine Scanning and Site-directed Mutagenesis. *J. Phys. Chem. B* **2010**, *114* (16), 5605−5616.
(48) (a) *SiteMap*, version 2.5; Schrödinger, LLC: New York, 2011. (b) Halgren, T. New Method for Fast and Accurate Binding-site Identification and Analysis. *Chem. Biol. Drug Des.* **2007**, *69*, 146−148. (c) Halgren, T. Identifying and Characterizing Binding Sites and Assessing Druggability. *J. Chem. Inf. Model.* **2009**, *49*, 377−389.